

# Photoinduced nonadiabatic dynamics in quartet Na<sub>3</sub> and K<sub>3</sub> formed using helium nanodroplet isolation

J. H. Reho,<sup>a)</sup> J. Higgins,<sup>b)</sup> M. Nooijen, K. K. Lehmann,<sup>c)</sup> and G. Scoles  
*Department of Chemistry, Princeton University, Princeton, New Jersey 08544*

M. Gutowski

*Battelle, Pacific Northwest National Laboratory, Richland, Washington 99352,  
and Department of Chemistry, University of Gdańsk, PL-80952, Gdańsk, Poland*

(Received 2 May 2001; accepted 24 September 2001)

Helium nanodroplet isolation is used to produce van der Waals-bound quartet state alkali trimers (Na<sub>3</sub> and K<sub>3</sub>) selectively over the corresponding chemically bound doublet trimers. Frequency-resolved excitation and emission spectroscopy reveals the presence of nonadiabatic spin-flip processes in the electronically excited states. A total of four quartet to quartet electronic transitions are observed: the  $2^4E', 1^4E \leftarrow 1^4A'_2$  transitions of Na<sub>3</sub> and the  $1^4A''_1, 2^4E' \leftarrow 1^4A'_2$  transitions of K<sub>3</sub>. Time-resolved spectroscopy reveals that intersystem crossing times in Na<sub>3</sub> decrease from 1.4 ns after excitation of the 0–0 band to approximately 400 ps for the higher vibronic levels (3,5/2). Analysis of the resonant quartet fluorescence reveals that the excited electronic state cools vibrationally on a time scale that is comparable to, but slower than, the intersystem crossing time. © 2001 American Institute of Physics. [DOI: 10.1063/1.1418248]

## I. INTRODUCTION

Recently, it has been shown in our laboratory that a beam of helium nanodroplets can be used in conjunction with a low density pick-up (scattering) cell to form the weakly bound, spin polarized, quartet trimers of sodium<sup>1–3</sup> and potassium.<sup>4</sup> While the chemically bound doublet states of Na<sub>3</sub> have been the object of many experimental<sup>5–12</sup> and computational<sup>13–15</sup> studies, no alkali metal quartet trimers had been previously observed. In the molecular beam spectrometer, when three randomly oriented gas-phase Na atoms are picked up by the same nanodroplet, they may combine to form Na<sub>3</sub> in either the doublet or the quartet spin state. While the abundance based upon spin statistics would be equal numbers of doublets and quartets, it has been observed in our laboratory that, downstream of the pick-up point, high-spin alkali oligomers are detected in much greater abundance than their low-spin counterparts.<sup>16</sup>

This selection of high-spin species can be understood considering the binding energies released upon formation of high- and low-spin Na<sub>3</sub>. In the formation of doublet Na<sub>3</sub>, approximately 8000 cm<sup>-1</sup> of energy (the binding energy of doublet Na<sub>3</sub> relative to three ground state sodium atoms) needs to be dissipated by the droplet through the evaporation of helium atoms. As each helium atom is bound to the droplet by  $\sim 5$  cm<sup>-1</sup>, a substantial percentage of a  $\langle N \rangle = 10^3 - 10^4$  helium nanodroplet (the droplet size range typically used to form these species) would be destroyed through this process. Furthermore, because of the weak alkali–

helium interaction energy,<sup>17</sup> the Na atoms reside on the surface<sup>18</sup> where they meet to form trimers and undergo vibrational relaxation (cooling). However, relaxation-induced droplet evaporation of the trimer may also occur, with consequent loss of doublet trimer–nanodroplet complexes. Instead, upon formation of quartet Na<sub>3</sub>, which is bound by only 850 cm<sup>-1</sup>, only a small percentage of helium in a nanodroplet would need to be evaporated to cool the trimer and the droplet to the 0.38 K<sup>19</sup> terminal temperature of the latter. A comparison of the two processes is shown schematically in Fig. 1. The droplets that need to dissipate the chemical energy liberated in the doublet trimer formation have a lower probability of survival, as shown by the fact that doublet trimer spectra have not been detected. The nanodroplets that bear the quartet trimers, however, do survive and are detected. Thus the selection of high-spin oligomers by helium nanodroplets is explainable by energetic considerations similar to those that justify why their formation in standard molecular beam experiments is so unlikely.

In the previous work that was conducted in our laboratory,<sup>3</sup> quartet trimers of Na<sub>3</sub> and K<sub>3</sub> formed using the helium nanodroplet isolation technique were used to investigate a unimolecular reaction where the bonding nature of the van der Waals-bound quartet trimers is converted to covalent following electronic excitation. In this paper, frequency-resolved spectra of two quartet transitions (one each in Na<sub>3</sub> and K<sub>3</sub>) will be presented in addition to those that had been previously reported. We will extend the Jahn–Teller analysis performed for the  $2^4E' \leftarrow 1^4A'_2$  transition of Na<sub>3</sub> to the case of quartet K<sub>3</sub>. Time-resolved experiments will be presented which provide quantitative dynamical data on the nonadiabatic spin-flip process that takes place in the excited quartet state of Na<sub>3</sub>. The analysis of the resonant emission of the  $2^4E' \rightarrow 1^4A'_2$  transition of Na<sub>3</sub>, which was first reported in a

<sup>a)</sup>Present address: Department of Chemistry, East Carolina University, East Fifth Street, Greenville, NC 27858.

<sup>b)</sup>Present address: Merck Research Laboratories, Merck & Co. Inc., P.O. Box 4, WP78-110 West Point, PA 19486.

<sup>c)</sup>Electronic mail: lehmann@princeton.edu

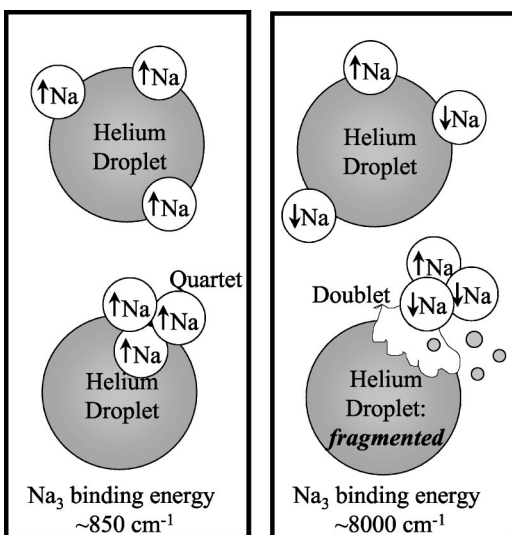


FIG. 1. Schematic representation of the formation of sodium quartet trimer (left panel) and doublet trimer (right panel) on the surface of a helium nanodroplet. In the former case, the trimer is likely to remain on the helium nanodroplet while in the latter case the trimer-droplet complex is not likely to survive.

previous publication by the authors,<sup>2,4</sup> had suggested the presence of vibrational cooling of the excited state by the host helium nanodroplet. Here we will present a quantitative analysis of the time-resolved resonant emission from which the lifetimes for vibrational relaxation in the  $2^4E'$  excited state of  $\text{Na}_3$  will be extracted.

## II. EXPERIMENT

The production and use of helium nanodroplets as a matrix for spectroscopic experiments is made possible by a molecular beam apparatus that is described hereafter. The helium nanodroplet source consists of a nozzle of either 10 or 20  $\mu\text{m}$  diameter cooled to 14–25 K. Through this nozzle helium gas is expanded at a pressure of 5.4 MPa, generating a beam of nanodroplets that passes through a 400  $\mu\text{m}$  skimmer into a pick-up cell where it interacts with a low pressure vapor (0.01–0.2 Pa) of the alkali metal of interest. The alkali metal atoms that collide with a helium nanodroplet become attached to it and can subsequently be used for spectroscopic study. After doping, the nanodroplets encounter the laser interaction area that is located 3.5 cm ( $\sim 90 \mu\text{s}$  flight time) downstream from the pick-up cell. The probe laser beam enters the vacuum apparatus through a baffle and crosses the molecular beam at  $90^\circ$  in the center of a laser-induced fluorescence (LIF) collector.

The LIF collector is comprised of an elliptical and a spherical mirror which surround the molecular and laser beam interaction region and coincide with one focus of the elliptical mirror and the center of the spherical mirror. The other focus of the elliptical mirror lies at the entrance to a 6-mm-diam incoherent multimode optical fiber bundle that is located on the surface of the spherical mirror and transports the photons to the appropriate detector. Such a two-mirror design is capable of collecting over 80% of the photons generated in the interaction region (although a lower fraction of

photons actually arrives at the detector due to the properties of our collection fiber bundle). However, this efficiency is reduced by approximately a factor of 2 when the spherical mirror is replaced by a flat black-coated substitute. This substitution, and the consequent loss in collection efficiency, is required for the time-resolved photon counting experiments to be described in the following because the presence of the spherical mirror would allow for two pathways differing in time by  $\sim 400$  ps through which photons can gain access to the fiber bundle.

Frequency-resolved spectra of the alkali-doped helium nanodroplets were obtained using either a continuous wave (cw) Coherent 699-21 dye laser incorporating DCM (14 500–16 800  $\text{cm}^{-1}$ ) laser dye or a cw Schwartz-EO Ti:Al<sub>2</sub>O<sub>3</sub> laser. Two sets of optics were employed in the Ti:Al<sub>2</sub>O<sub>3</sub> laser: a short band set in the range of 12 195–14 285  $\text{cm}^{-1}$  and a midband set between 11 049 and 14 184  $\text{cm}^{-1}$ . The linewidth of the Coherent 699 dye laser was determined to be less than 0.1  $\text{cm}^{-1}$  while the effective linewidth of the Ti:Al<sub>2</sub>O<sub>3</sub> laser was 0.25  $\text{cm}^{-1}$ . A home-built wavemeter was used to measure the frequency of the lasers. The accuracy of the wavemeter is determined to be better than 0.01  $\text{cm}^{-1}$  by recording the spectrum of I<sub>2</sub>. The main portion of the laser output was directed into a single-mode optical fiber and transported to the input of the molecular beam apparatus. Fluorescence photons were detected by a photomultiplier tube (ThorEMI 9863QB) operated in a pulse-counting mode. Emission spectra were obtained by imaging the fluorescence from the optical fiber bundle onto the entrance slit of a 0.35 m monochromator (MacPherson EU-700). A liquid nitrogen-cooled charged coupled device (Princeton Instruments 1152UV) was used to acquire the emission spectra.

For the time-resolved experiments, a mode-locked, doubled Coherent Antares Nd:YAG laser producing a pulse train with a frequency of 76 MHz at 532 nm was used as the pump laser. The typical average output power of the second harmonic was kept at or under 2 W. This green pulse train synchronously pumps one or both of two Coherent 700 folded-cavity dye lasers. Each dye laser is equipped with a cavity dumper (Coherent 7210). Typically the system was operated so as to produce extra-cavity pulses with a frequency of 3.8 MHz. Typical values for the average power of the dye laser output at a 76 MHz repetition rate (running R6G dye at 589 nm) are around 300 mW, which corresponds to about 4 nJ of energy per pulse, while the average output power of 120 mW attainable with the 3.8 MHz repetition rate by use of the cavity dumper in the pulsed mode corresponds to pulse energies of about 30 nJ.

The reversed time-correlated photon counting apparatus used in our laboratory has been described elsewhere.<sup>20</sup> Reversed time-correlated photon counting is employed in order to take advantage of a greater laser repetition rate while assuring the absence of temporal bias in the data. The time resolution of a time-correlated single photon counting instrument is empirically determined through the collection of an instrument response function.<sup>21</sup> The instrument response function is obtained with a pure scattering experiment in which the finite rise (and width) of the collected pulse rep-

resents the finite rise time (and jitter) of the electronic instruments employed in the experiment.<sup>22</sup> Our instrument response function was obtained by producing a beam of hydrogen aggregates through a 30 K nozzle and was found to have a full width at half maximum (FWHM) of  $\sim 200$  ps. The time resolution, however, is not limited by the FWHM of the instrument response function but rather by the jitter of its rising edge. Thus a factor of one-tenth of the FWHM of the instrument response function in time is often taken as the limit of temporal resolvability of a time-correlated single photon counting instrument.<sup>23</sup>

Modeling of the time-resolved data is carried out through an iterative convolution method written using the MATHCAD<sup>24</sup> suite of programs. The numerical instrument function is convoluted with a kinetic model by use of a pair of fast Fourier transforms using the following kinetic model:

$$G(t) = A(e^{-t/\tau_1} - e^{-t/\tau_2}) + D \quad (1)$$

in which  $\tau_2$  and  $\tau_1$  represent the rise and fall times, respectively, of the fluorescing species.  $D$  accounts for dark counts in the multichannel detector. The amplitude  $A$  as well as the exponential arguments  $\tau_i$  are parameters in a weighted least-squares fit to the observed decay curve. A weighting factor of  $1/N_i$  is used to weight each bin in accordance with Poisson statistics where  $N_i$  is the observed number of counts in the  $i$ th bin. The global minimum of  $\chi^2$  is sought through the Marquardt algorithm. This fitting method avoids the problems of noise amplification otherwise prevalent in the deconvolution of a response function from the experimental histogram by Fourier transform methods.<sup>25</sup>

### III. FREQUENCY-RESOLVED EXCITATION AND EMISSION SPECTRA OF QUARTET STATE ALKALI TRIMERS

#### A. Excitation spectra

Figure 2(a) shows the  $2^4E' \leftarrow 1^4A_2'$  excitation spectrum of Na<sub>3</sub> on helium nanodroplets obtained with a mean droplet size of approximately 11 000 helium atoms produced at a stagnation pressure of 5.4 MPa and a nozzle temperature of 17.5 K through a 10  $\mu$ m nozzle. The LIF excitation spectrum was obtained using the Coherent 699 cw dye laser.

In order to assign the excited electronic states of both Na<sub>3</sub> and K<sub>3</sub> (see the following), the experimental transition frequencies are compared to those obtained from *ab initio* calculations using multireference configuration interaction (MRCI)<sup>3</sup> and the equation of motion coupled cluster technique with single and double excitations (EOM-CCSD).<sup>26</sup> Table I displays the energies and symmetries of the calculated electronic states of Na<sub>3</sub> using both techniques. All energies correspond to the vertical transition from the lowest quartet state to the electronically excited state shown in Table I. As can be seen from Table I, the spectrum of quartet Na<sub>3</sub> that is shown in Fig. 2(a) corresponds to the second dipole allowed transition (to a  $2^4E'$  state). The calculated transition wave number found using both MRCI (15 461  $\text{cm}^{-1}$ ) and CCSD (15 872  $\text{cm}^{-1}$ ) are both very close to the observed value of 15 817  $\text{cm}^{-1}$ .

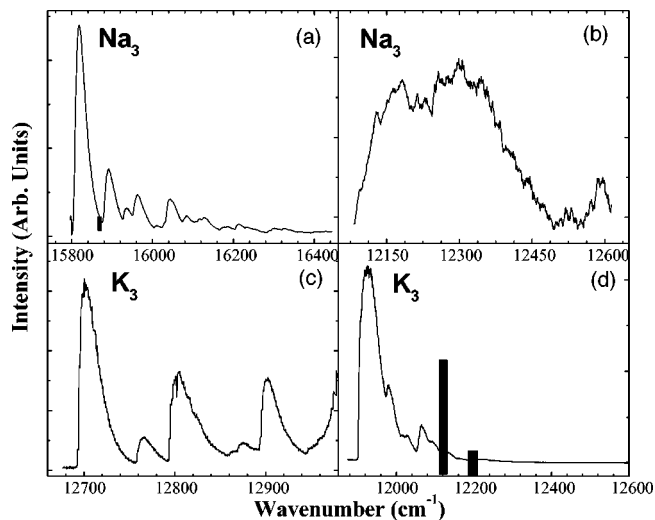


FIG. 2. Excitation spectra of quartet transitions of Na<sub>3</sub> and K<sub>3</sub>. (a) The  $2^4E' \leftarrow 1^4A_2'$  transition of Na<sub>3</sub>. (b) The  $1^4E' \leftarrow 1^4A_2'$  transition of Na<sub>3</sub>. (c) Excitation spectrum of the  $1^4A_1'' \leftarrow 1^4A_2'$  (tentative assignment) transition of K<sub>3</sub>. (d) Excitation spectrum of the  $2^4E' \leftarrow 1^4A_2'$  transition of K<sub>3</sub>. The solid bars indicate the prediction of the EOM-CCSD calculations which in the case of K<sub>3</sub> have been scaled.

It has been reported prior to this work<sup>3,4</sup> that quartet trimers of Na and K, upon electronic excitation, can undergo curve crossing into the doublet manifold. After crossing into the doublet manifold, the molecule will be in an excited state that is expected to dissociate into an atom and a covalently bound singlet dimer. Evidence for this simple unimolecular reaction has been found through the dispersed emission spectra collected upon  $2^4E' \leftarrow 1^4A_2'$  excitation of Na<sub>3</sub> that is reproduced<sup>3,4</sup> in Fig. 3(a). The arrow in Fig. 3(a) represents the frequency position of the excitation laser. As seen from Fig. 3(a), aside from the slightly redshifted resonant emission (marked 1) there are two spectral features at higher energy than the excitation wavelength. The feature marked 2

TABLE I. Calculated excitation energies in the quartet manifold of Na<sub>3</sub>. The highlighted states are those that have been observed using the helium nanodroplet isolation technique.

State (dominant excitation)	Excitation energy ( $\text{cm}^{-1}$ ) (MRCI) <sup>a</sup>	Excitation energy ( $\text{cm}^{-1}$ ) (EOMCCSD) <sup>b</sup>	Dipole allowed	Oscillator strength
$1^4A_2''$	0	0		
$1^4E''[e' > a_2'']$	10 433	10 047	Forbidden	0
$1^4A_1'[e' > e']$	11 434	11 927	Forbidden	0
<b><math>1^4E'[e' &gt; a_1']</math></b>	<b>12 219</b>	<b>12 387</b>	<b>Allowed</b>	<b>0.4/0.32</b>
$2^4A_2'[e' > e']$	13 460	13 322	Forbidden	0
<b><math>2^4E'[e' &gt; e']</math></b>	<b>15 461</b>	<b>15 872</b>	<b>Allowed</b>	<b>0.5/0.61</b>
$2^4E''[e' > e'']$	18 275	18 549	Forbidden	0
$1^4A_1''[e' > e'']$	18 965	19 409	Allowed	0.85/0.75
$1^4A_2''[e' > e'']$	19 855	...	Forbidden	0
$3^4E'$	20 874	21 617	Allowed	0.02/0.014
$3^4A_2'$	21 514	...	Forbidden	0
$3^4E''$	22 862	...	Forbidden	0
$4^4E'$	...	22 254	Allowed	0.014
$2^4A_1''$	...	25 805	Allowed	0.22

<sup>a</sup>Reference 3.

<sup>b</sup>Reference 26.

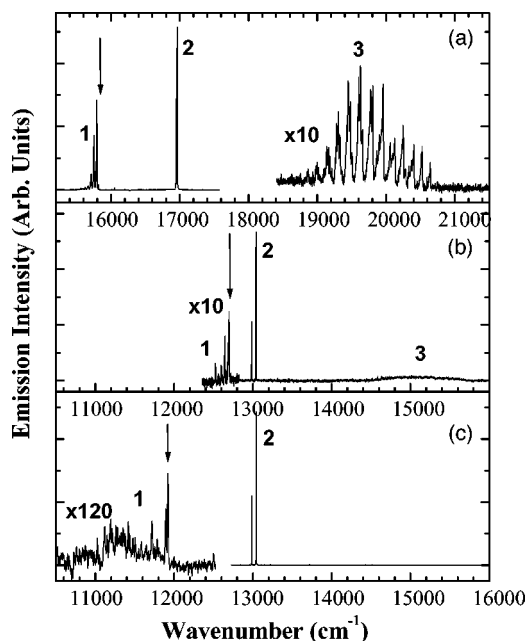


FIG. 3. Dispersed emission spectra of the quartet transitions of  $\text{Na}_3$  and  $\text{K}_3$ . The excitation is indicated by the arrow in each panel. (a) Emission spectrum obtained upon  $2^4E' \leftarrow 1^4A_2'$  excitation of  $\text{Na}_3$ . 1: Resonant  $2^4E' \rightarrow 1^4A_2'$  emission. 2: Na atomic  $3^2P_{3/2,1/2} \rightarrow 3^2S_{1/2}$  emission. 3:  $\text{Na}_2(B)1^1\Pi_u \rightarrow (X)1^1\Sigma_g^+$  emission. (b) Emission spectrum of the  $1^4A_1'' \rightarrow 1^4A_2'$  transition (tentative assignment) of  $\text{K}_3$ . 1: Resonant  $1^4A_1'' \rightarrow 1^4A_2'$  emission. 2: K atomic  $4^2P_{3/2,1/2} \rightarrow 4^2S_{1/2}$  emission. 3:  $\text{K}_2(B)1^1\Pi_u \rightarrow (X)1^1\Sigma_g^+$  emission. (c) Emission spectrum of the  $2^4E' \rightarrow 1^4A_2'$  transition of  $\text{K}_3$ . 1: Resonant  $2^4E' \rightarrow 1^4A_2'$  emission of  $\text{K}_3$ . 2: K atomic  $4^2P_{3/2,1/2} \rightarrow 4^2S_{1/2}$  emission.

in Fig. 3(a) corresponds to the  $3^2P_{3/2,1/2} \rightarrow 3^2S_{1/2}$  atomic emission of Na, and the feature marked 3 is assigned to the  $(B)1^1\Pi_u \rightarrow (X)1^1\Sigma_g^+$  transition of singlet  $\text{Na}_2$ . Neither of these higher-energy features is the result of a multiple photon excitation process (as the intensities scale linearly with laser power) and thus each is the product of the intersystem crossing of  $\text{Na}_3$  into a predissociative doublet state. Figure 4 illustrates schematically the three possible decay channels of  $\text{Na}_3$  which become open after  $2^4E' \leftarrow 1^4A_2'$  excitation.

In addition to the observation of the  $2^4E' \leftarrow 1^4A_2'$  transition of  $\text{Na}_3$  that was recorded near  $15800\text{ cm}^{-1}$ , an excitation spectrum of Na-doped helium nanodroplets acquired using the  $\text{Ti}:\text{Al}_2\text{O}_3$  laser operating in the short wavelength

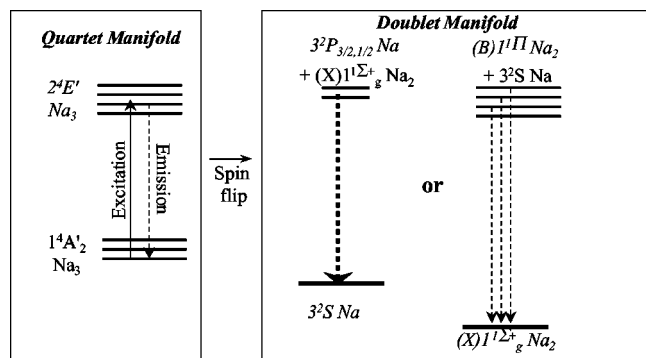


FIG. 4. Schematic representation of the evolution of the electronically excited quartet  $\text{Na}_3$  after excitation of the  $2^4E' \leftarrow 1^4A_2'$  transition.

band revealed a broad absorption between  $12000$  and  $12500\text{ cm}^{-1}$  [see Fig. 2(b)]. There is no resolved vibronic structure present and the overall intensity of the band is much weaker than that of the  $2^4E' \leftarrow 1^4A_2'$  transition in  $\text{Na}_3$ . Due to the weak intensity of this transition, an emission spectrum could not be obtained. The excitation spectrum can, however, be assigned to the  $1^4E' \leftarrow 1^4A_2'$  quartet transition of  $\text{Na}_3$  by comparison to the *ab initio* calculations shown in Table I. The MRCI calculation predicts a  $1^4E'$  state at  $12219\text{ cm}^{-1}$  above the lowest quartet state, while the EOM-CCSD calculation predicts a transition at  $12387\text{ cm}^{-1}$ , both in very close agreement with the observed transition. The spectrum lacks a strong 0–0 transition, which is an indication that there is a large geometry change upon excitation to the excited state. The Franck–Condon envelope of the transition is therefore spread out in frequency and the vibronic structure becomes “washed out” as the individual lines overlap due to the broadening induced by the helium nanodroplet.

As in the case of sodium, the collection of three K atoms with parallel electron spins allows for the formation of a quartet potassium trimer on the nanodroplet surface. It can be reasonably assumed that the energies of the excited electronic states of the alkali dimers and trimers scale in an approximate way with the energy of the corresponding atomic excitations. While the Na atomic  $3^2P_{3/2} \leftarrow 3^2S_{1/2}$  transition lies at  $16973.4\text{ cm}^{-1}$ , the corresponding K transition ( $4^2P_{3/2} \leftarrow 4^2S_{1/2}$ ) occurs at  $13042.9\text{ cm}^{-1}$ . Following this scaling, the transitions from the  $1^4A_2'$  lowest quartet state to the  $1^4E'$ ,  $2^4E'$ , and  $1^4A_1''$  states of  $\text{K}_3$  should be found at the following approximate wave numbers:  $9500$ ,  $12200$ , and  $14900\text{ cm}^{-1}$ , respectively.

The first quartet  $\text{K}_3$  transition, observed by scanning the  $\text{Ti}:\text{Al}_2\text{O}_3$  laser from  $11900$  to  $12400\text{ cm}^{-1}$ , agrees with the second predicted frequency and is displayed in Fig. 2(d). By comparison with the calculated electronic states of the sodium trimer, this transition can be identified as the  $2^4E' \leftarrow 1^4A_2'$  transition of  $\text{K}_3$ . A scan at higher frequencies reveals a second  $\text{K}_3$  quartet transition with an origin at  $12690\text{ cm}^{-1}$ , which is partially masked by the excitation spectrum of potassium atoms on the helium nanodroplets [see Fig. 2(c)]. For this experiment, the potassium oven was maintained at a temperature of  $174^\circ\text{C}$ . A  $10\text{ }\mu\text{m}$  nozzle cooled to a temperature of  $17.5\text{ K}$  and a helium stagnation pressure of  $5.4\text{ MPa}$  (average droplet size— $11000$  atoms/droplet) was used to produce the helium nanodroplet beam. To confirm the assignment to a potassium trimer transition, an alkali metal pressure dependence of the LIF signal was recorded and displays an initial cubic dependence that is expected for a transition originating from a trimer.<sup>27</sup> This transition is, however, not in coincidence with any of the three frequencies predicted previously. Following the scaling of the  $\text{Na}_3$  quartet transitions, the next higher dipole allowed transition after the  $2^4E' \leftarrow 1^4A_2'$  would be a  $1^4A_1'' \leftarrow 1^4A_2'$  transition. Based upon this scaling, we tentatively assign the spectrum beginning at  $12690\text{ cm}^{-1}$  [shown in Fig. 2(c)] to a  $1^4A_1'' \leftarrow 1^4A_2'$  transition of  $\text{K}_3$ . With  $4A_1''$  symmetry of the excited state, a strong vibronic progression of the  $\nu_1$  mode (symmetric stretch,  $a_1'$  symmetry in the  $D_{3h}$  configuration) in the spectrum of the  $\text{K}_3$  transition shown in Fig. 2(c) can be as-

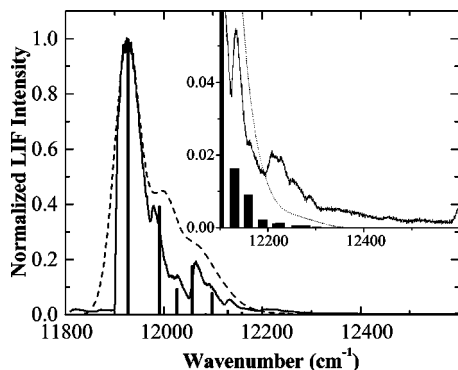


FIG. 5. Comparison of experimental (solid line) and calculated (solid bars) spectrum of the  $2^4E' \leftarrow 1^4A_2'$  transition of  $K_3$  using a linear plus quadratic Jahn–Teller model. The dashed line is a convolution of the calculated transitions with a Gaussian line shape of  $57 \text{ cm}^{-1}$  width. The inset is an expanded view of the region from  $12100$  to  $12600 \text{ cm}^{-1}$ .

signed to the prominent peaks at  $12702$ ,  $12802$ , and  $12904 \text{ cm}^{-1}$ . This yields a  $\nu_1$  frequency of approximately  $100 \text{ cm}^{-1}$ . The weaker bands observed in the  $K_3$  spectrum can therefore be assigned to a weak progression of even quanta in  $\nu_2$ , which has  $e'$  symmetry.

Let us now return to the comparison between the  $2^4E' \leftarrow 1^4A_2'$  spectra of  $Na_3$  and  $K_3$ . Both spectra are dominated by a 0–0 band with large intensity and accompanied at higher energy by a weaker vibronic progression of the Jahn–Teller active mode.<sup>2</sup> The vibronic bands in the  $K_3$  spectrum are not as well resolved as those of the  $Na_3$  spectrum due to several factors. The broadening in the  $K_3$  spectrum ( $57 \text{ cm}^{-1}$ ) is slightly greater than that observed in  $Na_3$  ( $29 \text{ cm}^{-1}$ , FWHM of 0–0 band). This is probably due to a greater coupling of the trimer to the internal modes of the helium nanodroplet. Also, the heavier atomic mass of potassium results in lower vibrational frequencies of the  $K_3$  molecule than that of  $Na_3$ , leading to a closer spacing between lines. The excitation spectrum of this transition of  $K_3$  can be assigned using the  $E \otimes e$  Jahn–Teller coupling model employing the same procedure as was used for the assignment of the  $Na_3$  spectrum.<sup>2</sup> Figure 5 displays the experimental spectrum and the calculated levels that result from a fit to the linear and quadratic Jahn–Teller coupling parameters. The calculated spectrum is convoluted with a Gaussian line shape of  $57 \text{ cm}^{-1}$  width for comparison to the experimental spectrum. The parameters of the Jahn–Teller analysis are listed in Table II, comparing them to the results for the  $2^4E' \leftarrow 1^4A_2'$  transition of  $Na_3$ .

TABLE II. Jahn–Teller parameters of the  $2^4E'$  state of  $Na_3$  and  $K_3$ .

Molecule	Parameter	Value ( $\text{cm}^{-1}$ )
$Na_3$	Asymmetric stretch ( $\nu_2$ )	88.2
	Linear Jahn–Teller coupling ( $k$ )	63.5
	Quadratic Jahn–Teller coupling ( $g$ )	42.3
$K_3$	Asymmetric stretch ( $\nu_2$ )	67.9
	Linear Jahn–Teller coupling ( $k$ )	57.0
	Quadratic Jahn–Teller coupling ( $g$ )	23.1

TABLE III. Experimental and calculated peak positions of the  $2^4E' \leftarrow 1^4A_2'$  transition of  $K_3$ .

Quantum numbers ( $v, j$ )	Experiment ( $\text{cm}^{-1}$ )	Calculated ( $\text{cm}^{-1}$ )	Difference ( $\text{cm}^{-1}$ )
(0,0) origin	11 927.08	11 927.08	0.00
(1,1/2)	11 979.74	11 991.12	−11.38
(2,5/2)	12 027.28	12 026.76	0.52
(2,1/2)	12 065.19	12 057.40	7.79
(3,7/2)	12 085.16	12 084.74	0.42
(3,1/2)	12 092.51	12 097.96	−5.45
(3,5/2)	12 132.95	12 130.32	2.63
(4,5/2)	12 162.61	12 158.88	3.73
(4,1/2)	12 189.64	12 173.5	16.14
(4,7/2)	12 196.36	12 189.07	7.29
(5,11/2)	12 211.02	12 217.99	−6.97
(5,7/2)	12 228.40	12 225.65	2.75
(5,1/2)	12 239.94	12 243.92	−3.98
(6,13/2)	12 252.12	12 258.45	−6.33
(6,5/2)	12 264.05	12 263.02	1.03
(6,1/2)	12 287.13	12 279.92	7.51
(6,7/2)	12 302.51	12 301.67	0.84

The linear Jahn–Teller coupling, normalized to the frequency of the asymmetric vibration, is similar in the  $2^4E'$  state of  $K_3$  (0.84) and the  $2^4E'$  state of  $Na_3$  (0.72), leading to a Jahn–Teller stabilization energy that is almost identical in the two molecules ( $24 \text{ cm}^{-1}$  in  $K_3$ ,  $22 \text{ cm}^{-1}$  in  $Na_3$ ). The normalized quadratic coupling in  $K_3$  (0.34) is lower than that of  $Na_3$  (0.48), producing a smaller barrier between the three local minima of the  $D_{3h}$  molecule. Table III lists the positions of the experimental and calculated vibronic bands of the  $2^4E' \leftarrow 1^4A_2'$  transition of  $K_3$  on the helium nanodroplet surface.

## B. Emission spectra

The emission spectra of the two quartet transitions of  $K_3$  provide valuable data on the nonadiabatic spin–flip processes that occur in the quartet trimer. In addition, analysis of the resonant fluorescence allows a detailed study of the lowest quartet state of the trimer. Figure 3(b) displays an emission spectrum obtained by exciting the  $1^4A_1'' \leftarrow 1^4A_2'$  transition of  $K_3$  with the  $Ti:Al_2O_3$  laser positioned at  $12700.6 \text{ cm}^{-1}$ . The spectrum is similar to that obtained by the excitation of the  $2^4E' \leftarrow 1^4A_2'$  transition of  $Na_3$  because inter-system crossing of the quartet state places the trimer in an excited doublet state that predissociates into an atom and singlet dimer. Also in this case three channels of fluorescence are observed in exact accordance with the  $Na_3$  spectrum, two of which are at higher energy than the excitation energy. The group of lines near region 1 in the spectrum is the resonant  $1^4A_1'' \rightarrow 1^4A_2'$  deexcitation back to the lowest quartet state of  $K_3$ . The fluorescence at points 2 and 3 is emission from the dissociation products of the doublet potassium trimer. As the electronic excitation can be localized on either product, the fluorescence at point 2 arises from the atomic  $K 4^2P_{3/2,1/2} \rightarrow 4^2S_{1/2}$  transition, and the fluorescence at point 3 results from the  $(B)1^1\Pi_u \rightarrow (X)1^1\Sigma_g^+$  transition of singlet  $K_2$ . Accurate vibrational frequencies for the lowest quartet state can

TABLE IV. Experimental peak positions of the  $1^4A_1' \rightarrow 1^4A_2'$  transition (tentative assignment) of  $K_3$ .

Peak number	Position ( $\text{cm}^{-1}$ )
1	12 688
2	12 646
3	12 600
4	12 563
5	12 526

be extracted from the resonant fluorescence to the  $1^4A_2'$  state of  $K_3$  (peak positions are reported in Table IV). These could be compared to calculated frequencies employing an *ab initio* potential surface that, however, in the case of  $K_3$  is substantially more difficult to calculate precisely than in the case of quartet  $Na_3$ .<sup>1</sup>

The emission spectrum obtained by exciting the  $2^4E' \leftarrow 1^4A_2'$  transition of  $K_3$  at  $11\,925.8\text{ cm}^{-1}$  (peak of the 0–0 band) is displayed in Fig. 3(c). Only two channels of fluorescence are found instead of three. The most prominent feature in the spectrum is the  $4^2P_{3/2,1/2} \rightarrow 4^2S_{1/2}$  atomic transition of potassium. A very minor component of the fluorescence is seen below  $12\,000\text{ cm}^{-1}$  and corresponds to the resonant quartet fluorescence. Also in this case intersystem crossing into the doublet manifold of the trimer is occurring as was observed in the other quartet transitions observed in  $Na_3$  and  $K_3$ . The branching ratio for the product fluorescence after spin-flip is however quite different upon excitation of the  $2^4E' \leftarrow 1^4A_2'$  transition as all of the fluorescence is localized on the atomic potassium fragment. Several factors can affect the intersystem crossing rate in the  $2^4E' \leftarrow 1^4A_2'$  transition of  $K_3$ . Since the Jahn–Teller parameters and the magnitude of the  $\nu_2$  vibrational frequency are comparable in the  $2^4E'$  state of both  $Na_3$  and  $K_3$ , similar potential surface gradients near the doublet-quartet state crossing would lead to an increased rate of intersystem crossing. In addition, the spin–orbit coupling matrix element is expected to be greater in  $K_3$  than in  $Na_3$ , which would lead to greater fluorescence in the doublet dissociation channels. However, since the form of the doublet potential surface to which the quartet state is coupled is unknown, it is not possible to evaluate the effect of these differences with any amount of confidence.

## IV. TIME-RESOLVED STUDIES

### A. Intersystem crossing dynamics

The intersystem crossing of  $Na_3$  from the quartet to the doublet manifold is an example of a unimolecular reaction of a triatomic complex in which spectroscopic information from the product channels can be obtained. The case of the quartet alkali trimers is particularly interesting, as the bonding nature of the products differs from that of the reactant. In order to gain a more complete understanding of the reaction dynamics of this system, time-resolved studies have been carried out on quartet  $Na_3$  in which measurements have been made of product-channel fluorescence onset and decays.

Our time-resolved studies employ the time-correlated single photon counting system described in Sec. II. Measure-

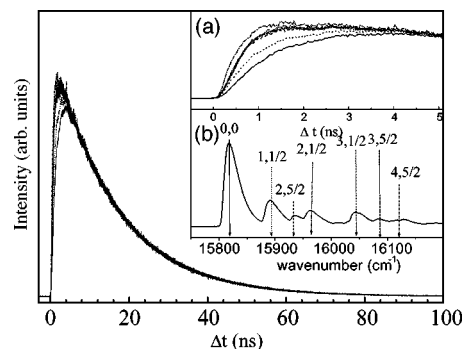


FIG. 6. Time-resolved Na atomic  $3^2P \rightarrow 3^2S$  fluorescence collected upon  $2^4E' \leftarrow 1^4A_2'$  excitation of  $Na_3$ . (a) The fluorescence onsets of each of the spectra are highlighted. (b) The excitation spectrum with arrows indicating the excitations used in collection of the time-resolved spectra.

ments were made by inserting an Andover 589FS-10 band-pass filter between the excitation and detection regions in order to selectively collect fluorescence arising from the atomic dissociation product only. Thus, both the singlet dimer emission and the resonant quartet-to-quartet fluorescence were completely suppressed. As shown in Fig. 6(a) the fluorescence rise times become faster for excitations of higher  $2^4E'$  vibronic trimer bands. The fluorescence plots shown in the Fig. 6 are normalized for sake of comparison. The excitation frequencies are shown in Fig. 6(b), where they are labeled by  $\nu, j$  quantum numbers of the initially populated vibronic levels. The line types used for the identification arrows of the excitation frequencies correspond to the line types used in the fluorescence plots shown in Fig. 6(a). Modeling this data using a single exponential rise and single exponential fall time yields good fits. The results of these fits are given in Table V. It is found from Table V that the measured fall times reproduce the known gas phase literature values of the lifetime of Na  $3^2P$  state,<sup>28</sup> confirming that the spin-flip products emit as gas phase species and highlighting the relative accuracy of our photon counting instrument.

TABLE V. Onset times for Na singlet dimer [ $(B)1^1\Pi_u \rightarrow (X)1^1\Sigma_g^+$ ] and Na atomic ( $3^2P_{3/2,1/2} \rightarrow 3^2S_{1/2}$ ) fluorescence generated upon excitation of the  $\nu, j$  bands of the  $2^4E'$  state of  $Na_3$ . The lifetime for the  $3^2P$  state of Na is the average of the  $3^2P_{1/2}$  and  $3^2P_{3/2}$  states as reported in Ref. 28.

$\nu, j$	Rise times ( $\pm 50$ ps)		Fall times ( $\pm 0.1$ ns)	
	Na dimer ( $B \rightarrow X$ )	Na atom ( $P \rightarrow S$ )	Na dimer ( $B \rightarrow X$ )	Na atom ( $P \rightarrow S$ )
0,0	1425	1435	6.65	16.28
1,1/2	940	940	6.65	16.26
2,5/2	427	445	6.65	16.28
2,1/2	382	438	6.68	16.24
3,1/2	370	417	6.67	16.29
3,5/2	385	434	6.64	16.28
4,5/2	222	345	6.65	16.26
Average lifetime			6.66	16.27
Experimental lifetime <sup>a</sup>			7	16.23

<sup>a</sup>References 28 and 30.

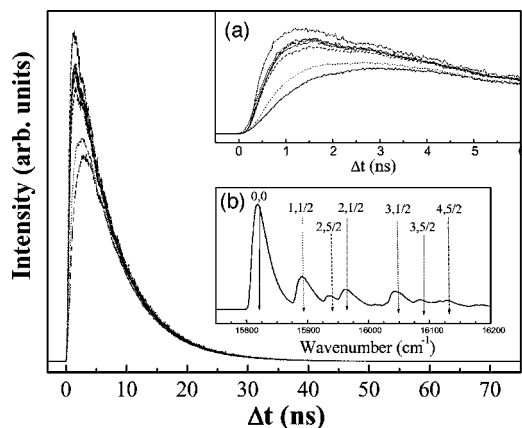


FIG. 7. Time-resolved  $(B)1^1\Pi_u \rightarrow (X)1^1\Sigma_g^+$  fluorescence of Na<sub>2</sub> collected upon  $2^4E' \leftarrow 1^4A_2'$  excitation of Na<sub>3</sub>. (a) The fluorescence onsets of each of the spectra are highlighted. (b) The excitation spectrum with arrows indicating the excitations used in collection of the time-resolved spectra.

Figure 7 shows the normalized plot of the Na<sub>2</sub>  $(B)1^1\Pi_u \rightarrow (X)1^1\Sigma_g^+$  product fluorescence obtained upon  $2^4E' \leftarrow 1^4A_2'$  excitation of Na<sub>3</sub>. Selective photon collection was accomplished by use of an Andover 500FS-10 bandpass filter, which effectively suppresses all but the fluorescence emanating from the dimer product. The results of the best fits to the data are given in Table V. From Fig. 7 and Table V it can again be seen that the onset of product fluorescence occurs more quickly as the energy of excitation increases. The positions of the excitation energies are shown in Fig. 7 as an inset, with line types of the arrows corresponding to the fluorescence plots. Excepting the case corresponding to the highest energy excitation, the fluorescence onset times of the atom and dimer products are quite similar, as for all but the highest-energy excitation, the rise times of the dimer spin-flip product and the atom spin-flip product fall within the reported error (see Table V). We also note the fast decrease in fluorescence onset time for the first few excitation energies and the ensuing plateau of onset times (again excepting the last point).

The fluorescence onset time of the emission products represents the time needed to populate the Na<sub>2</sub>  $(B)1^1\Pi_u \rightarrow (X)1^1\Sigma_g^+$  and the Na atomic  $3^2P_{3/2,1/2} \rightarrow 3^2S_{1/2}$  emission channels. The time taken to populate these channels is a sum of the time needed for intersystem crossing of the vibronically excited Na<sub>3</sub> from the quartet to doublet manifold and the time needed for dissociation of the predissociative doublet into the gas-phase dimeric and atomic fluorescence products. As the time spent in the predissociative doublet state is expected to be negligible (i.e., a few picoseconds), it is reasonable to equate the fluorescent onset times of the dimeric and atomic emission products with the actual intersystem crossing time. Thus the times reported in Table V represent the lifetimes of intersystem crossing for particular vibronic bands of the sodium quartet trimer.

We then find that for excitations of the lowest (0,0)  $2^4E'$  band of Na<sub>3</sub>, intersystem crossing occurs in roughly 1.4 ns, while this time shrinks to around 400 ps for the higher ( $v=3$ ) bands. Radiative decay of the quartet state can be estimated to be 19.5 ns based on the oscillator strength

estimated by the MRCI method. We have also found that the branching ratio between the spin-flip products is constant as a function of the excitation energy.<sup>4</sup> The emission spectra of the singlet dimer obtained upon excitation of the (0,0) band and the (1,1/2) band of the excited quartet trimer yield indistinguishable intensity patterns. This is consistent with the model of intersystem crossing into the doublet state that will occur at a specific energy through a “doorway” state. Once the intersystem crossing occurs, the trimer will arrive at the same configuration on the potential energy surface irrespective of the level excited in the quartet system. This in turn will lead to identical product distributions that are not dependent on the excitation energy.

This being the case, it is possible to conclude that the electronically excited quartet trimer accesses a single window into the doublet manifold. If multiple access points to the doublet manifold were attainable at the excitations studied here, the product branching ratios (which would be different for different intersystem crossing windows) would be found to differ as a function of excitation energy. The energy at which this curve crossing occurs appears to be located near  $16050 \pm 50 \text{ cm}^{-1}$  above the lowest level of the  $1^4A_2'$  state.

## B. Time-resolved $2^4E' \rightarrow 1^4A_2'$ resonant emission of Na<sub>3</sub>

The strongest fluorescence of the resonant  $2^4E' \rightarrow 1^4A_2'$  emission occurs at  $15792 \text{ cm}^{-1}$ , which represents a  $35 \text{ cm}^{-1}$  shift to the red of the (0,0)  $2^4E' \leftarrow 1^4A_2'$  Na<sub>3</sub> excitation. Evidence for vibrational cooling of the excited quartet state comes from collection of the  $2^4E' \rightarrow 1^4A_2'$  resonant fluorescence upon excitation of the higher  $v, j$  bands of the  $2^4E'$  state. Excitation of the (1,1/2), (2,5/2), (2,1/2), and (3,1/2) yields emissions which are dominated by progressions of transitions that begin near the wave number of the (0,0) vibronic level of the  $2^4E'$  state. Some emission from higher  $2^4E'$  vibronic levels is observed (to higher energies than the 0–0 transition at  $15792 \text{ cm}^{-1}$ ), but this only constitutes a minor component of the total emission. Thus the dispersed emission spectra indicate that there is vibrational cooling of higher  $v, j$  bands of the  $2^4E'$  state of Na<sub>3</sub>.

The  $2^4E' \rightarrow 1^4A_2'$  resonant emission from Na<sub>3</sub> was time resolved using reverse time-correlated single photon counting to obtain information on the vibrational cooling rates. A bandpass filter (Andover 633FS10-50) is used to selectively collect the resonant fluorescence and to suppress any fluorescence generated from the excitation laser itself as well as fluorescence from the intersystem crossing products described previously. The width of this filter, however, was not narrow enough to discriminate among the various vibronic bands of the resonant fluorescence. That is, emission from all vibronic bands of the  $2^4E'$  state is passed with equal (minimal) suppression through the filter. Therefore, each measurement should contain lifetime components corresponding to not only the initially populated  $2^4E'$  pseudo-rovibrational level, but also to  $2^4E'$  levels of lower energy that become populated upon vibrational relaxation on the surface of the helium nanodroplet. Depopulation of the vibronically excited  $v, j$

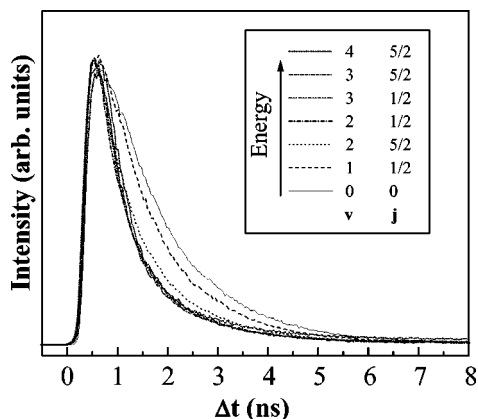


FIG. 8. Time-resolved  $2^4E' \rightarrow 1^4A_2'$   $\text{Na}_3$  fluorescence collected upon excitation of various (shown in the inset) pseudo-rovibrational levels of the  $\text{Na}_3$   $2^4E'$  state.

states of  $\text{Na}_3$  occurs through intersystem crossing, spontaneous emission, and vibrational cooling of the trimer. Thus, in analyzing the data, quantifying the fall time components for the higher-lying bands becomes difficult and we shall restrict the discussion to the resonant emission bands of lowest energy.

The temporal behavior of the resonant  $\text{Na}_3$  emission was studied for excitations of several  $2^4E'$  vibronic bands. These results are given in Fig. 8. It is seen from Fig. 8 that the fluorescence falls off more quickly as the excitation energy is increased. The fluorescence onset is instrument limited at  $\leq 50$  ps. Thus in the fitting of the fluorescence fall times described in the following, the fluorescence onset time is held constant at 20 ps. Fits employing other fixed rise times (50 and 5 ps) do not yield fall times which differ outside of the error of the  $\tau_{\text{rise}}=20$  ps fit. Thus a single, 20 ps rise time is employed in all fits to the fluorescence decays that follow.

A fit to the (0,0) emission yields a lifetime value of  $1.3 \pm 0.1$  ns. The model used for this fit is comprised of a (constant) instrumentally limited rise time and a single exponential fall. This model yields a single fall time of  $1.1 \pm 0.1$  ns for excitation of the (1,1/2) level, and 870 ps for the (2,5/2) level. The fits to the emission from the (0,0) and (1,1/2) bands are in reasonable agreement with the lifetimes deduced for the product rise times, while the fit for the (2,5/2) band is quite different. In the fits to the (1,1/2) and (2,5/2) bands using a single exponential fall, the reduced  $\chi^2$  was rather high (1.5 and higher) and so the data were reanalyzed using a multiple exponential model. For the (1,1/2) level the following model for the fall times, in which the fall time fit to the (0,0) level is included in the first term,<sup>29</sup> was used:

$$Ae^{-0.772t} + Be^{-k_{\text{fall}}t} \quad (2)$$

in which  $A$  and  $B$  are amplitude parameters and  $k_{\text{fall}}$  an additional fall rate parameter. The results from this fit are given in Table VI under the Multiple lifetime column. For the emission following excitation of the (2,5/2) level of  $\text{Na}_3$ , Eq. (2) was appended with an additional component:

TABLE VI. Fits to the lifetimes of the resonant emission of  $\text{Na}_3$ . The *Single lifetime* column represents the best fit to the data with a single exponential fall, which proved satisfactory only in the (0,0) case. The *Multiple lifetimes* column shows the results of fits to the data using models with multiple exponential fall times as discussed in the text.

Excited $2^4E'$ level	Single lifetime ( $\pm 0.1$ ns)	Multiple lifetimes (% total area)
(0,0)	1.30 ns	1.30 ns (100%)
(1,1/2)	1.10 ns	1.30 ns (65%) 0.89 ns (35%)
(2,5/2)	0.87 ns	1.30 ns (58%) 0.89 ns (2%) 0.57 ns (40%)

$$Ae^{t/1.296} + Be^{t/0.894} + Ce^{t/\tau_{\text{fall}}} \quad (3)$$

from which the new fall component  $\tau_{\text{fall}}$  was found to be 570 ps, as shown in Table VI.

For the (1,1/2) level, the kinetic equations used to model the measured lifetimes contain the following three rates:  $k_1$ =total depopulation rate for the (1,1/2) state including both electronic and vibrational relaxation;  $k_0$ =total depopulation rate for the (0,0) state by electronic deexcitation;  $k_{10}$ =population transfer rate from the (1,1/2) state to the (0,0) state.

Electronic deexcitation includes both intersystem crossing and radiative decay of the excited electronic state. Due to the low temperature of the helium nanodroplet relative to the vibrational spacings, we can neglect all up pumping processes. Upon optical excitation at time zero, we have  $P_1(0)=1$  and  $P_0(0)=0$ , where  $P_i(t)$  is the population of state  $i$  at time  $t$ . For  $t>0$ , we have the following solutions to the kinetic equations satisfying these initial conditions:

$$P_1(t) = e^{-k_1 t}, \quad (4)$$

$$P_0(t) = \frac{k_{10}}{k_1 - k_0} (e^{-k_0 t} - e^{-k_1 t}). \quad (5)$$

If we further assume that the rate of radiative decay is the same for both states, we get the time dependent total emission as

$$P_{\text{tot}}(t) = P_1(t) + P_0(t) = \left[ 1 - \left( \frac{k_{10}}{k_1 - k_0} \right) \right] e^{-k_1 t} + \left( \frac{k_{10}}{k_1 - k_0} \right) e^{-k_0 t}. \quad (6)$$

If we compare this with the values reported in Table VI, we can conclude that

$$k_{10} = 0.65(k_1 - k_0) = 0.226 \text{ ns}^{-1},$$

$$\tau_{10} = 4.42 \text{ ns},$$

where  $\tau_{10}$  is the lifetime for vibrational relaxation from the (1,1/2) to (0,0) levels. Thus 65% of the increased decay rate for the (1,1/2) level is due to vibrational relaxation to the (0,0) level, while 35% is due to increased electronic deexcitation, i.e., spin-orbit mixing. These rates can be compared to the rates  $k_1 = 0.893 \text{ ns}^{-1}$  and  $k_0 = 0.772 \text{ ns}^{-1}$ . Thus the vibrational relaxation from this lowest excited level is slower

but comparable with the nonradiative decay. The radiative decay rate calculated from the *ab initio* oscillator strength is 19.5 ns, which is a factor of 4.4 slower than the lifetime for vibrational relaxation from the (1,1/2) to (0,0) levels.

For excitation of the (2,5/2 band), there are now three additional rates in the kinetic model:  $k_2$ =total decay rate of state 2, the (2,5/2 state);  $k_{21}$ =population transfer rate from state 2 to state 1 (1,1/2);  $k_{20}$ =population transfer rate from state 2 to state 0 (0,0).

Also, we have the initial conditions  $P_2(0)=1$  and  $P_1(0)=P_0(0)=0$ . The solutions to the kinetic equations are

$$P_2(t) = e^{-k_2 t}, \quad (7)$$

$$P_1(t) = \frac{k_{21}}{k_2 - k_1} (e^{-k_1 t} - e^{-k_2 t}), \quad (8)$$

$$P_0(t) = A e^{-k_2 t} + B e^{-k_1 t} + C e^{-k_0 t}, \quad (9)$$

$$P_{\text{tot}}(t) = P_2(t) + P_1(t) + P_0(t), \quad (10)$$

where

$$A = \frac{-k_{20}}{k_2 - k_0} + \frac{k_{21} k_{10}}{(k_2 - k_0)(k_2 - k_1)},$$

$$B = \frac{-k_{21} k_{10}}{(k_1 - k_0)(k_2 - k_1)},$$

$$C = -A - B.$$

Note that the expressions for  $P_2$  and  $P_1$  are the same as for  $P_1$  and  $P_0$  given previously with a change of the labels. If we assume the values for the rates  $k_1$ ,  $k_0$ , and  $k_{10}$  from the earlier level, we can determine  $k_2$  from the new decay rate, and the two constants  $k_{21}$  and  $k_{20}$  from the relative amplitudes of the three exponential terms in  $P_{\text{total}}$ . From the 0.02 amplitude for the  $k_1$  term [taken from Table VI for excitation of the (2,5/2) level],  $k_{21}=0.022 \text{ ns}^{-1}$  and  $\tau_{21}=45.5 \text{ ns}$ , which is a minor relaxation channel. From the amplitude of 0.58 for the  $k_0$  term,  $k_{20}=0.555 \text{ ns}^{-1}$  and  $\tau_{20}=1.80 \text{ ns}$  for vibrational relaxation. This gives the electronic decay rate of state 2 as  $k_2 - k_{21} - k_{20} = 1.177 \text{ ns}^{-1}$  and a lifetime of 0.85 ns. Again, vibrational relaxation is not faster than the intersystem crossing rate.

If the vibrational relaxation was much faster than the electronic decay, then almost all the observed emission would be from the (0,0) level, regardless of which vibrational level was pumped, and then the observed time decay would be dominated by an exponential with a decay rate equal to that of the (0,0) level. The fact that for the higher levels the effective decay rate becomes considerably shorter means that only a small portion of the population relaxes to the (0,0) level of the excited electronic state.

## V. CONCLUSIONS

Quartet alkali trimers are a good example of the versatility of helium nanodroplet isolation for the formation of unusual van der Waals complexes and novel radical species. The low temperature (0.38 K)<sup>19</sup> and superfluid nature of the nanodroplets allows for the acquisition of electronic spectra of the quartet alkali trimers with vibrational resolution. Fur-

thermore, the van der Waals complex of three parallel spin alkali atoms acts as a precursor for a photoinitiated reaction that produces a covalently bound product by way of a nonadiabatic process in the excited quartet electronic state. This reaction can be analyzed in great detail because of the selective preparation of the initial state by the excitation laser and because precise energetic information on the product channels can be obtained through emission spectroscopy. A total of four quartet electronic transitions have been observed: the  $2^4E', 1^4E' \leftarrow 1^4A'_2$  transitions of Na<sub>3</sub> and the  $1^4A'_1, 2^4E' \leftarrow 1^4A'_2$  transitions of K<sub>3</sub>. A comparison of the product branching ratios between Na<sub>3</sub> and K<sub>3</sub> displays the effect of increased spin-orbit coupling in K<sub>3</sub> on the spin-flip process.

This system provides a unique opportunity to perform time-resolved measurements of covalent bond formation from a van der Waals-bound precursor. Using the technique of reverse time-correlated photon counting, we have found that the spin-flip process occurs in 1.4 ns for the 0-0 transition of Na<sub>3</sub>, decreasing to approximately 380 ps at the access point to the doublet manifold in the excited state. A single access point is inferred in the excited  $2^4E'$  electronic state of Na<sub>3</sub>. The magnitude of the rise times of the product fluorescence indicate that the quartet trimer is undergoing many vibrational oscillations in the excited state before a valence electron may undergo a spin-flip. With each crossing of the trimer through the intersection of the quartet and doublet potential energy surfaces, there is only a small probability of electron spin-flip. Time-resolved measurements of the resonant quartet fluorescence show that vibrational cooling of the excited electronic state occurs on a time scale somewhat slower than that of the spin-flip process. We have shown that the decay of the resonant fluorescence is limited by the spin-flip process and, upon an analysis that also accounts for the vibrational relaxation, yields similar rates for intersystem crossing as those measured by the rise time of the product fluorescence.

## ACKNOWLEDGMENTS

We are grateful for the help of Carlo Callegari in these experiments and we would like to acknowledge Wolfgang Ernst for useful discussions. M.G. acknowledges support from the DOE Office of Science, Division of Chemical Sciences. This work was carried out with the support of the AFOSR (HEDM program) under Grant No. F49620-95-10086.P0001.

<sup>1</sup>J. Higgins, T. Hollebeek, J. Reho, T.-S. Ho, K. K. Lehmann, H. Rabitz, G. Scoles, and M. Gutowski, *J. Chem. Phys.* **112**, 5751 (2000).

<sup>2</sup>J. Higgins, W. E. Ernst, C. Callegari, J. Reho, M. Gutowski, K. K. Lehmann, and G. Scoles, *Phys. Rev. Lett.* **77**, 4532 (1996).

<sup>3</sup>J. Higgins, C. Callegari, J. Reho, F. Stienkemeier, W. E. Ernst, K. K. Lehmann, M. Gutowski, and G. Scoles, *Science* **273**, 629 (1996).

<sup>4</sup>J. Higgins, Doctoral dissertation, Princeton University, 1998.

<sup>5</sup>E. Schreiber *et al.*, *Chem. Phys. Lett.* **242**, 106 (1995).

<sup>6</sup>M. Broyer, G. Delacrétaz, P. Labastie, J. P. Wolfe, and L. Wöste, *Phys. Rev. Lett.* **57**, 1851 (1986).

<sup>7</sup>M. Broyer *et al.*, *Phys. Rev. Lett.* **62**, 2100 (1989).

<sup>8</sup>C. R. Wang, S. Pollack, D. Cameron, and M. M. Kappes, *J. Chem. Phys.* **93**, 3787 (1990).

<sup>9</sup>B. Bühler, R. Thalweiser, and G. Gerber, *Chem. Phys. Lett.* **188**, 590 (1992).

- <sup>10</sup>H.-J. Foth, J. N. Gress, Chr. Hertzler, and W. Demtröder, *Z. Phys. D: At., Mol. Clusters* **18**, 257 (1991).
- <sup>11</sup>M. Meyer zur Heide, E. Tiemann, and D. Wendlandt, *Chem. Phys. Lett.* **199**, 590 (1992).
- <sup>12</sup>W. E. Ernst and S. Rakowsky, *Phys. Rev. Lett.* **74**, 58 (1995).
- <sup>13</sup>V. Bonačić-Koutecky, P. Fantucci, and J. Koutecky, *Chem. Rev.* **91**, 1035 (1991).
- <sup>14</sup>F. Cocchini, T. H. Upton, and W. Andreoni, *J. Chem. Phys.* **88**, 6068 (1988).
- <sup>15</sup>T. C. Thompson, G. Izmirlan, Jr., S. J. Lemon, D. G. Truhlar, and C. A. Mead, *J. Chem. Phys.* **82**, 5597 (1985).
- <sup>16</sup>J. Higgins, C. Callegari, J. Reho, W. E. Ernst, K. K. Lehmann, and G. Scoles, *J. Phys. Chem. A* **102**, 4952 (1998).
- <sup>17</sup>J. Pascale, *Technical Report, Service de Physique des Atoms et des Surfaces* (C. E. N. Saclay, Gif sur Yvette-Cédex, France, 1983).
- <sup>18</sup>F. Ancilotto, E. Cheng, M. W. Cole, and F. Toigo, *Z. Phys. B: Condens. Matter* **98**, 823 (1995).
- <sup>19</sup>M. Hartmann, R. E. Miller, J. P. Toennies, and A. Vilesov, *Phys. Rev. Lett.* **75**, 1566 (1995).
- <sup>20</sup>J. Reho, J. Higgins, K. K. Lehmann, and G. Scoles, *J. Chem. Phys.* **113**, 9694 (2000).
- <sup>21</sup>Hammamatsu Technical Service Note No. 50, 1987.
- <sup>22</sup>D. V. O'Connor and D. Phillips, *Time-correlated Single Photon Counting* (Academic, San Diego, 1984).
- <sup>23</sup>S. Cova, M. Ghioni, and F. Zappa, *Rev. Sci. Instrum.* **62**, 2596 (1991).
- <sup>24</sup>MATCAD PLUS 6.0. Mathsoft, Inc. 1996.
- <sup>25</sup>A. J. Cross and G. R. Fleming, *Biophys. J.* **46**, 45 (1984); D. V. O'Connor, W. R. Ware, and J. C. Andre, *J. Phys. Chem.* **83**, 1333 (1979).
- <sup>26</sup>J. F. Stanton and R. J. Bartlett, *J. Chem. Phys.* **98**, 7029 (1993); R. J. Bartlett and J. F. Stanton, *Rev. Comput. Chem.* **5**, 65 (1994).
- <sup>27</sup>F. Stienkemeier, J. Higgins, W. E. Ernst, and G. Scoles, *Z. Phys. B: Condens. Matter* **98**, 413 (1995).
- <sup>28</sup>E. B. Saloman, *Spectrochim. Acta, Part B* **48**, 1139 (1993).
- <sup>29</sup>This fit was first done using a biexponential fall model in which both fall rates were free parameters. The result of this calculation was that ~65% of the total emission was fit to a fall rate of  $0.667 \text{ ns}^{-1}$  (1.5 ns fall time), close to that measured for the (0,0) band. As this calculation was slow in converging, and as keeping three fall parameters free [for the (2,5/2) band] was not possible, it was decided that each successive component should remain fixed in the following calculation.
- <sup>30</sup>W. Demtröder, W. Setzenbach, M. Stock, and J. Wit. *J. Mol. Spectrosc.* **61**, 382 (1976).